Non-Model-Based Identification of Delamination in Laminated Composite Plates Using a Continuously Scanning Laser Doppler Vibrometer System

Da-Ming Chen
Department of Mechanical Engineering,
University of Maryland, Baltimore County,
1000 Hilltop Circle,
Baltimore, MD 21250

Y. F. Xu
Department of Mechanical and
Materials Engineering,
University of Cincinnati,
Cincinnati, OH 45221

W. D. Zhu[1]
Department of Mechanical Engineering,
University of Maryland, Baltimore County,
1000 Hilltop Circle,
Baltimore, MD 21250
e-mail: wzhu@umbc.edu

Delamination frequently occurs in a laminated composite structure and can cause prominent local anomalies in curvature vibration shapes associated with vibration shapes of the composite structure. Spatially dense vibration shapes of a structure can be rapidly obtained by use of a continuously scanning laser Doppler vibrometer (CSLDV) system, which sweeps its laser spot over a vibrating surface of the structure. This paper introduces a continuous scanning scheme for general quadrangular scan areas assigned on plates and extends two damage identification methods for beams to identify delamination in laminated composite plates using a CSLDV system. One method is based on the technique that a curvature vibration shape from a polynomial that fits a vibration shape of a damaged structure can well approximate an associated curvature vibration shape of an undamaged structure and local anomalies caused by structural damage can be identified by comparing the curvature vibration shape of the damaged structure with that from the polynomial fit, and the other is based on the technique that a continuous wavelet transform can directly identify local anomalies in a curvature vibration shape caused by structural damage. The two methods yield corresponding damage indices and local anomalies in curvature vibration shapes can be identified in neighborhoods with high damage index values. Both numerical and experimental investigations on effectiveness of the two methods are conducted on a laminated composite plate with a delamination area. In the experimental investigation, delamination identification results from the two methods were compared with that from a C-scan image of the composite plate.
[DOI: 10.1115/1.4038734]

Keywords: laminated composite plate, delamination identification, wavelet transform, polynomial fit, continuously scanning laser Doppler vibrometer system

1 Introduction

Among various types of structural damage, delamination is one that frequently occurs in laminated composite structures. Since delamination is usually hidden from external view, it can be difficult to identify. When delamination occurs, local stiffness of a laminated composite structure in neighborhoods of the delamination can change and modal parameters of the structure, including natural frequencies, modal damping ratios and mode shapes, can subsequently change [1–3]. Effects of delamination on modal parameters of composite structures have been studied with their analytical, semi-analytical, and finite element models [4–6]. Specifically, vibration shapes, such as mode shapes and operating deflection shapes, have been widely used for structural damage identification since spatial derivatives of vibration shapes, such as curvature vibration shapes [7] and slope vibration shapes [8], better manifest local anomalies caused by the damage, and identification methods that use curvature vibration shapes of laminated composite structures have been developed [3,9,10]. A polynomial-based method was proposed in Ref. [7], where curvature mode shapes of damaged and undamaged beams are compared and damage can be identified in neighborhoods with large differences between them. In the polynomial-based method, a curvature vibration shape of an undamaged beam is not needed as it is obtained from a polynomial that fits a vibration shape of a damaged beam; the method was extended to identify damage in plates using vibration shapes measured in a point-by-point manner by a scanning laser Doppler vibrometer [11]. A wavelet-based method was proposed in Ref. [8], where slope vibration shapes of damaged beams are wavelet-transformed and damage can be identified in neighborhoods with large wavelet-transform coefficients. The polynomial- and wavelet-based methods inspect smoothness of vibration shapes of beams by identifying prominent local anomalies in curvature and slope vibration shapes caused by damage, and they can be extended to identify delamination in laminated composite plates, since delamination can also cause local anomalies in curvature vibration shapes of plates.

A laser Doppler vibrometer is capable of accurate, noncontact surface vibration measurement thanks to Doppler shifts between the incident light from and scattered light back to the vibrometer [12]. A laser Doppler vibrometer becomes a scanning laser Doppler vibrometer when equipped with a scanner that consists of a pair of orthogonal scan mirrors and its laser beam can be directed to any position visible to the scanner. However, point-by-point acquisition of a vibration shape of a large-sized structure with a dense measurement grid can be time-consuming even though it can be achieved in an automatic and well-controlled manner. The idea of continuous scanning was first proposed in Refs. [13] and [14], where a scanning laser Doppler vibrometer continuously sweeps its laser spot over a surface of a structure under sinusoidal excitation to obtain its vibration shapes that are approximated by

[1]Corresponding author.

Contributed by the Technical Committee on Vibration and Sound of ASME for publication in the Journal of Vibration and Acoustics. Manuscript received August 11, 2017; final manuscript received December 7, 2017; published online February 22, 2018. Assoc. Editor: Huageng Luo.

Chebyshev series. Two vibration shape measurement methods for continuous scanning, including demodulation and polynomial methods, were later proposed in Refs. [15–17]. The demodulation method was extended for structures under impact and multisine excitation in Refs. [18] and [19], respectively. A lifting method was proposed to obtain mode shapes of a structure under impact excitation by treating its free response measured by a continuously scanning laser Doppler vibrometer (CSLDV) system as that of a linear time-periodic system [20]. The demodulation and polynomial methods were synthesized to identify damage in beams, where damage behind an intact surface of a beam could be identified by use of a CSLDV system that scanned the intact surface [21]. A new type of vibration shapes called free-response shapes was developed and a corresponding damage identification method was proposed to identify damage in beams undergoing free vibration [22]. Damage indices associated with multiple elastic modes of beams can be obtained in one measurement by a CSLDV system and damage can be identified near neighborhoods with consistently high damage index values.

In this work, the polynomial- and wavelet-based identification methods are extended from beam damage identification to laminated composite plate delamination identification using a CSLDV system. A continuous scanning scheme is developed for general quadrangular scan areas assigned on a plate. A vibration shape of a plate is formed by vibration shapes along straight scan paths spanning a scan area assigned on the plate. Damage indices on each scan path from the two methods constitute corresponding damage indices of a whole plate and edges of delamination areas can be identified near neighborhoods with high damage index values. Effectiveness of the two identification methods is numerically investigated with a finite element model of a composite plate with a delamination area. The composite plate was manufactured to experimentally investigate effectiveness of the two methods, and experimental delamination identification results were compared with that of a C-scan image of the plate.

2 Methodology

2.1 Damage Identification Using Curvature Vibration Shapes. A curvature vibration shape of a beam is the second-order spatial derivative of a vibration shape z along the direction of its length x', and it can be calculated using a central finite difference scheme

$$z_{x'x'}(x') = \frac{z(x'-h) - 2z(x') + z(x'+h)}{h^2} \tag{1}$$

where h is the distance between two neighboring measurement points of z along x'. Structural damage can cause local changes of bending stiffness of a beam EI. Since the relationship between $z_{x'x'}$ and EI can be expressed by [8]

$$z_{x'x'}(x') = \frac{M(x')}{EI(x')} \tag{2}$$

with M denoting the bending moment of the beam, prominent local anomalies can be observed in $z_{x'x'}$ in neighborhoods of the damage, and the damage can be identified by inspecting $z_{x'x'}$ for anomalies.

A similar relationship between bending stiffness of a plate $Eh^3/(12(\nu^2-1))$ and its curvatures along an arbitrary scan path of a CSLDV system, with x and y denoting its tangential and normal directions, respectively, can be expressed by [23]

$$\begin{bmatrix} M_{xx} \\ M_{yy} \end{bmatrix} = \frac{Eh^3}{12(\nu^2-1)} \begin{bmatrix} 1 & \nu \\ \nu & 1 \end{bmatrix} \begin{bmatrix} z_{xx} \\ z_{yy} \end{bmatrix} \tag{3}$$

where z_{xx} and z_{yy} denote curvatures of the plate along x and y, respectively; M_{xx}, $M_{yy,}$ and ν denote bending moments along x and y and Poison's ratio of the plate, respectively. As structural damage can cause changes to $Eh^3/(12(\nu^2-1))$, prominent local anomalies can be observed in neighborhoods of the damage, and the damage can be identified by inspecting z_{xx} and/or z_{yy}. Straight scan paths are assigned on a plate and its vibration shapes are formed by those along assigned straight scan paths on the plate. The central finite difference scheme in Eq. (1) can be applied to calculate z_{xx}, and it can be expressed by

$$z_{xx}(x) = \frac{z(x+h) - 2z(x) + z(x-h)}{h^2} \tag{4}$$

By assuming that measurement points on a straight scan path are equally spaced, the smaller h in Eq. (4) the more accurate the resulting z_{xx}, which is true when z is free of measurement noise. When z is contaminated by measurement noise, it can be expressed by

$$z(x) = z^{\mathrm{NF}}(x) + \sigma(x) \tag{5}$$

where z^{NF} and σ denote a noise-free vibration shape and measurement noise, respectively. Substituting Eq. (5) into Eq. (4) yields

$$\begin{aligned} z_{xx}(x) &= \frac{z^{\mathrm{NF}}(x+h) + \sigma(x+h) - 2z^{\mathrm{NF}}(x) - 2\sigma(x) + z^{\mathrm{NF}}(x-h) + \sigma(x-h)}{h^2} \\ &= \frac{z^{\mathrm{NF}}(x+h) - 2z^{\mathrm{NF}}(x) + z^{\mathrm{NF}}(x-h)}{h^2} + \frac{\sigma(x+h) - 2\sigma(x) + \sigma(x-h)}{h^2} \end{aligned} \tag{6}$$

When h is small, adverse effects of σ can be drastically amplified in the resulting z_{xx} due to the term $(\sigma(x+h) - 2\sigma(x) + \sigma(x-h))/h^2$ in Eq. (6). One can modify Eq. (4) by introducing a resolution parameter n

$$z_{xx}(x) = \frac{z(x+nh) - 2z(x) + z(x-nh)}{(nh)^2} \tag{7}$$

Substituting Eq. (5) into Eq. (7) yields

$$\begin{aligned} z_{xx}(x) &= \frac{z^{\mathrm{NF}}(x+nh) + \sigma(x+nh) - 2z^{\mathrm{NF}}(x) - 2\sigma(x) + z^{\mathrm{NF}}(x-nh) + \sigma(x-nh)}{(nh)^2} \\ &= \frac{z^{\mathrm{NF}}(x+nh) - 2z^{\mathrm{NF}}(x) + z^{\mathrm{NF}}(x-nh)}{(nh)^2} + \frac{\sigma(x+nh) - 2\sigma(x) + \sigma(x-nh)}{(nh)^2} \end{aligned} \tag{8}$$

By comparing the term $(\sigma(x+h)-2\sigma(x)+\sigma(x-h))/h^2$ in Eq. (6) and the term $(\sigma(x+nh)-2\sigma(x)+\sigma(x-nh))/(nh)^2$ in Eq. (8), one can see that adverse effects of measurement noise on z_{xx} can be alleviated in the latter by n^2 times due to introduction of n. A suitable value of n is the least one with which z_{xx} seems free of adverse effects of measurement noise and one can obtain such a value by increasing n from a small value and observing the resulting z_{xx}. When x in Eq. (4) is close to a boundary of z, $z(x+h)$ and $z(x-h)$ may not exist and the central finite difference scheme can fail. A mode shape extension technique was proposed in Ref. [7] to append virtual mode shape extensions to boundaries of a mode shape so that both $z(x+h)$ and $z(x-h)$ become available even when x in Eq. (4) is close to a boundary of z. The mode shape extension technique is applicable to an operating deflection shape.

2.2 Demodulation Method. Application of the demodulation method for obtaining a vibration shape along a straight scan path using a CSLDV system is summarized below. Steady-state response of a structure under sinusoidal excitation with a frequency f measured by a CSLDV system can be expressed by

$$r(t) = z(x(t))\cos(2\pi ft - \alpha - \theta) \tag{9}$$

where $x(t)$ denotes the spatial position of the laser spot from the CSLDV system on the structure, α is the difference between a phase determined by initial conditions of the structure and that determined by a mirror feedback signal, and θ is a phase variable that controls amplitudes of in-phase and quadrature components of z, which can be expressed by

$$z_I(x) = z(x)\cos(\alpha+\theta) \tag{10}$$

and

$$z_Q(x) = z(x)\sin(\alpha+\theta) \tag{11}$$

respectively [21]. Each obtained vibration shape from the demodulation method corresponds to a half-scan period. A half-scan period starts when the laser spot of the CSLDV system arrives at one end of a scan path and ends when the laser spot arrives at the other end. The steady-state response $r(t)$ in Eq. (9) can be further expressed by

$$r(t) = z_I(x(t))\cos(2\pi ft) + z_Q(x(t))\sin(2\pi ft) \tag{12}$$

Multiplying Eq. (12) by $\cos(2\pi ft)$ and $\sin(2\pi ft)$ yields

$$\begin{aligned} r(t)\cos(2\pi ft) &= z_I(x(t))\cos^2(2\pi ft) + z_Q(x(t))\sin(2\pi ft)\cos(2\pi ft) \\ &= \frac{1}{2}z_I(x(t)) + \frac{1}{2}z_I(x(t))\cos(4\pi ft) + \frac{1}{2}\phi_Q(x(t)) \\ &\quad \times \sin(4\pi ft) \end{aligned} \tag{13}$$

and

$$\begin{aligned} r(t)\sin(2\pi ft) &= z_I(x(t))\cos(2\pi ft)\sin(2\pi ft) + z_Q(x(t))\sin^2(2\pi ft) \\ &= \frac{1}{2}z_Q(x(t)) - \frac{1}{2}z_Q(x(t))\cos(4\pi ft) + \frac{1}{2}z_I(x(t)) \\ &\quad \times \sin(4\pi ft) \end{aligned} \tag{14}$$

respectively. A low-pass filter is applied to $r(t)\cos(2\pi ft)$ and $r(t)\sin(2\pi ft)$ to obtain $(1/2)z_I$ and $(1/2)z_Q$, respectively, and terms corresponding to the frequency $2f$ in Eqs. (13) and (14) can be removed. Further, z_I and z_Q can be obtained by multiplying the corresponding filtered response by two. The value of θ in Eq. (11) can be optimized so that z_I and z_Q attain their maximum and minimum amplitudes, respectively. In what follows, all vibration shapes from the demodulation method are presented as their in-phase components with maximum amplitudes, which are denoted by z for convenience.

2.3 Polynomial-Based Damage Identification. As mentioned in Sec. 2.1, damage can cause prominent local anomalies in curvature vibration shapes. Such anomalies can be identified by comparing curvature vibration shapes of undamaged and damaged structures. However, vibration shapes and curvature vibration shapes of undamaged structures are usually unavailable in practice. It was shown in Ref. [7] that curvature vibration shapes of an undamaged beam can be well approximated by those from polynomials that fit vibration shapes of a damaged beam outside their boundary regions. Though vibration shapes from polynomial fits may not satisfy boundary conditions of damaged and undamaged beams, curvature vibration shapes associated with the vibration shapes can be used for damage identification purposes outside boundary regions. The mode shape extension technique in Ref. [7] can yield curvature mode shapes from polynomial fits that well approximate those of whole undamaged beams. However, this technique is inapplicable to vibration shapes of beams that are obtained using the demodulation method, as their curvature vibration shapes have inherent local distortions near boundaries of scan paths [21]. Due to the same reason, the mode shape extension technique mentioned in Ref. [7] is not applicable to vibration shapes of plates. A polynomial that fits z of a damaged plate along a straight scan path with order r can be expressed by

$$z^{\mathrm{p}}(x) = \sum_{q=0}^{r} a_q x^q \tag{15}$$

where a_q are coefficients of the polynomial that can be obtained by solving a linear equation

$$\mathbf{U}\mathbf{a} = \mathbf{z} \tag{16}$$

in which $\mathbf{U}$ is an $M \times (r+1)$ Vandermonde matrix with M being the number of measurement points of z

$$\mathbf{U} = \begin{bmatrix} 1 & x_1 & x_1^2 & \cdots & x_1^r \\ 1 & x_2 & x_2^2 & \cdots & x_2^r \\ \vdots & \vdots & \vdots & \ddots & \vdots \\ 1 & x_M & x_M^2 & \cdots & x_M^r \end{bmatrix} \tag{17}$$

$\mathbf{a} = [\,a_0 \quad a_1 \quad \ldots \quad a_r\,]^{\mathrm{T}}$ is an $(r+1)$-dimensional coefficient vector, and $\mathbf{z}$ is the vibration shape vector to be fit. To avoid ill-conditioning of $\mathbf{U}$, it is proposed that x in Eq. (15) be normalized using the "center and scale" technique [24] before formulating the linear equation in Eq. (15). The normalized coordinate $\hat{x}$ can be expressed by

$$\hat{x} = \frac{2x - 2\bar{x}}{l} \tag{18}$$

where $\bar{x}$ is the x-coordinate of the center point of a straight scan path and l is its length.

In order to determine the proper value of r, a fitting index fit and a convergence index con can be used. Fitting index fit at r can be expressed by

$$\mathrm{fit}(r) = \frac{\mathrm{RMS}(\mathbf{z})}{\mathrm{RMS}(\mathbf{z}) + \mathrm{RMS}(\mathbf{e})} \times 100\% \tag{19}$$

where $\mathrm{RMS}(\cdot)$ denotes the root-mean-square value of a vector and $\mathbf{e} = \mathbf{U}\mathbf{a} - \mathbf{z}$ is an error vector. Convergence index con can be expressed by

$$\mathrm{con}(r) = \mathrm{fit}(r) - \mathrm{fit}(r-2) \tag{20}$$

where $r \geq 3$. When fit is close to 100%, z^{p} completely fits z; the lower fit, the lower the level of fitting of z^{p} to z. When con is close to 0, increasing r cannot further improve how well z^{p} fits z; the lower con, the higher the level of convergence of z^{p}. It is proposed in this work that the proper value of r be the minimum value of r with which $\mathrm{con}(r)$ is below 0.05%. When z^{p} is obtained from a polynomial with a proper order, a curvature damage index ρ can be defined along a straight scan path at x [7]

$$\rho(x) = |z_{xx}(x) - z^{\mathrm{p}}_{xx}(x)|^2 \tag{21}$$

and the damage can be identified in neighborhoods with high ρ. When ρ associated with n different vibration shapes is available, an auxiliary curvature damage index ρ_{a} is proposed

$$\rho_{\mathrm{a}}(x,y) = \sum \overline{\rho}_k(x,y) \tag{22}$$

where $\overline{\rho}_k$ is the normalized damage index associated with the kth available vibration shape, whose maximum index value is one, and Σ denotes summation over all available normalized damage indices. Due to inherent local distortions in curvature vibration shapes near boundaries of scan paths, only ρ outside boundary regions are considered for delamination identification purposes here.

2.4 Wavelet-Based Damage Identification. A wavelet transformation can be defined by

$$W_\psi z(u,s) = \int_{-\infty}^{+\infty} z(x)\psi^*_{u,s}(x)\mathrm{d}x \tag{23}$$

where W_ψ denotes a wavelet transformation operator with a wavelet function

$$\psi_{u,s}(x) = \frac{1}{\sqrt{s}}\psi\left(\frac{x-u}{s}\right) \tag{24}$$

in which u and s are spatial and scale parameters of $\psi_{u,s}$, respectively, and the superscript $*$ denotes complex conjugation. In this work, a wavelet function is defined in the real domain and the superscript $*$ in Eq. (23) can be dropped. The wavelet transformation in Eq. (23) can be expressed in the form of a convolution

$$W_\psi z(u,s) = \frac{1}{\sqrt{s}}\int_{-\infty}^{+\infty} z(x)\overline{\psi}\left(\frac{u-x}{s}\right)\mathrm{d}x = \frac{1}{\sqrt{s}} z \otimes \overline{\psi} \tag{25}$$

where an overbar denotes function reflection over the y-axis, i.e., $\overline{\psi}(x) = \psi(-x)$, and $\otimes$ denotes convolution.

The energy-normalized Gaussian function

$$g_0(x) = \left(\frac{2}{\pi}\right)^{\frac{1}{4}} e^{-x^2} \tag{26}$$

is used to generate Gaussian wavelet family for the wavelet transformation in this work due to its smoothness, differentiability, localization in the spatial domain and explicit mathematical expressions. The pth order Gaussian wavelet function can be expressed by

$$g_p(x) = (-1)^n \frac{d^p g_0(x)}{\mathrm{d}x^p} \tag{27}$$

In order to inspect vibration shapes for local anomalies caused by structural damage, g_2 is used in a wavelet transformation of $z_{xx}(x)$ that is expressed by

$$W_{g_2} z_{xx}(u,s) = \frac{1}{\sqrt{s}} z_{xx} \otimes \overline{g_2} \tag{28}$$

By the theorem of convolution differentiation [25], W_{g_2} in Eq. (28) can be further expressed by

$$W_{g_2} z_{xx}(u,s) = \frac{1}{\sqrt{s}} z \otimes \frac{d^2\overline{g_2}}{\mathrm{d}x^2} = \frac{1}{s^{\frac{5}{2}}} z \otimes \overline{g_4} \tag{29}$$

A wavelet damage index δ can be defined along a straight scan path at the location u with the scale s

$$\delta(u,s) = |W_{g_2} z_{xx}(u,s)|^2 = \left|\frac{1}{s^2} W_{g_4} z(u,s)\right|^2 \tag{30}$$

and damage can be identified near neighborhoods with high δ. When δ associated with n different vibration shapes is available, an auxiliary wavelet damage index δ_{a} is proposed

$$\delta_{\mathrm{a}}(x,y) = \sum \overline{\delta}_k(x,y) \tag{31}$$

where $\overline{\delta}_k$ is the normalized wavelet damage index associated with the kth available vibration shape, whose maximum index value is one.

3 Continuous Scanning Scheme for a Plate

A typical CSLDV system comprises of three key components, including a single-point laser Doppler vibrometer, a scanner, and a control unit that is a dSPACE MicroLabBox in this work, as shown in Fig. 1(*a*). The vibrometer measures the velocity along the direction of its laser beam at a measurement point where its

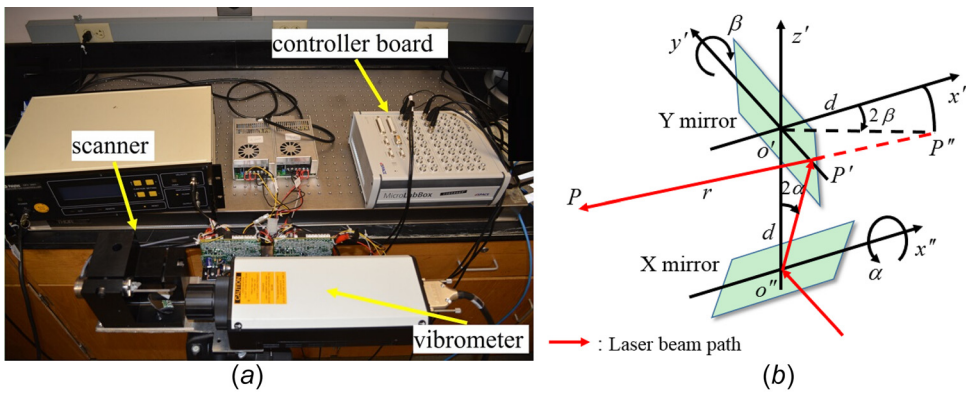

Fig. 1 (*a*) Components of a CSLDV system and (*b*) a simplified diagram of the CSLDV system

laser spot is located. The scanner directs the laser spot onto an assigned measurement point P [26], as shown in Fig. 1(*b*). The scanner has two orthogonal scan mirrors called X and Y mirrors, and rotation angles of the two mirrors are positioned by two independent stepper motors inside the scanner, which are controlled by the control unit. The X and Y mirrors control horizontal and vertical positions of the laser spot, respectively.

Various scan trajectories of the laser spot can be created by providing proper signals for the scanner via the control unit. Zigzag scan trajectories are generated to obtain vibration shapes of a plate in this work. A zigzag scan trajectory consists of straight scan paths that span an assigned quadrangular scan area, and a vibration shape of the plate is formed by its vibration shape along each scan path that is obtained from the demodulation method. An example of a zigzag scan trajectory that spans a rectangular scan area is shown in Fig. 2. The trajectory in Fig. 2(*a*) is called a horizontal scan trajectory as its scan paths span mainly in the horizontal direction, i.e., the x-direction. A counterpart of a horizontal scan trajectory is a vertical scan trajectory as shown in Fig. 2(*b*), which consists of straight scan paths spanning mainly in the vertical direction, i.e., the y-direction.

In a vibration shape of a beam, there is one value of each damage index that can be obtained at one point of the vibration shape, as the vibration can only be measured along one direction, i.e., along its length, by a CSLDV system. However, there can be countless values of each damage index that can be obtained at one point of a vibration shape of a plate measured by a CSLDV system, as the vibration shape of the plate at the point can be measured along countless directions. While horizontal and vertical scan trajectories are selected to form damage indices here, scan paths in a scan trajectory do not need to be horizontal or vertical, and they can be any smooth curves.

A continuous scanning scheme is introduced here to generate horizontal and vertical scan trajectories on a general quadrangular scan area as shown in Fig. 3. The quadrangular scan area is defined by four vertices P_{ll}, P_{lr}, P_{ul}, and P_{ur}, which correspond to its lower left, lower right, upper left, and upper right corners, respectively. Cartesian coordinate system is defined with P_{ll} as its origin. A mathematical description of the continuous scanning scheme to generate a horizontal scan trajectory is provided below.

Without loss of generality, the description is provided with voltage signals used as control variables, which is directly related to rotation angles of the two mirrors. Voltage signals provided for the X and Y mirrors corresponding to P_{ll}, P_{lr}, P_{ul}, and P_{ur} are $(\alpha_{ll}, \beta_{ll})$, $(\alpha_{lr}, \beta_{lr})$, $(\alpha_{ul}, \beta_{ul})$, and $(\alpha_{ur}, \beta_{ur})$, respectively, where α and β values denote voltage signals provided for the X and Y mirrors, respectively. Both lines $P_{ll}P_{ul}$ and $P_{lr}P_{ur}$ are evenly divided into $N-1$ parts by N numbered points, as shown in Fig. 3, and a total of $2N-1$ straight scan paths can be formed on the scan area. A straight scan path in the trajectory is formed by connecting one point on the line $P_{ll}P_{ul}$ and one on the line $P_{lr}P_{ur}$.

The increment of an α value from one numbered point to the next on the line $P_{ll}P_{ul}$ can be expressed by

$$\Delta\alpha_l = \frac{\alpha_{ul} - \alpha_{ll}}{N-1} \tag{32}$$

and that on the line $P_{lr}P_{ur}$ can be expressed by

$$\Delta\alpha_r = \frac{\alpha_{ur} - \alpha_{lr}}{N-1} \tag{33}$$

Averaging can improve signal-to-noise ratios of vibration shapes measured by a CSLDV system [26]. On each scan path of a scan trajectory, M end-to-end scans are performed before the laser spot scans the next scan path and a vibration shape along the scan path can be averaged from measurements from the M scans. The number of averages per scan path M is an odd number so that scanning of a scan path can start from one numbered point and end at the other. The α value for the ith scan path can be expressed by

$$\alpha_i = \begin{cases} [\alpha_{ll} + (i-1)\times\Delta\alpha_l] + k_{\alpha i}\times t, & i = 1, 3, \ldots, 2N-1 \text{ and } j = 1, 3, \ldots, M \\ (\alpha_{lr} + i\times\Delta\alpha_r) - k_{\alpha i}\times t, & i = 1, 3, \ldots, 2N-1 \text{ and } j = 2, 4, \ldots, M-1 \\ [\alpha_{lr} + (i-1)\times\Delta\alpha_r] + k_{\alpha i}\times t, & i = 2, 4, \ldots, 2N-2 \text{ and } j = 1, 3, \ldots, M \\ (\alpha_{ll} + i\times\Delta\alpha_l) - k_{\alpha i}\times t, & i = 2, 4, \ldots, 2N-2 \text{ and } j = 2, 4, \ldots, M-1 \end{cases} \tag{34}$$

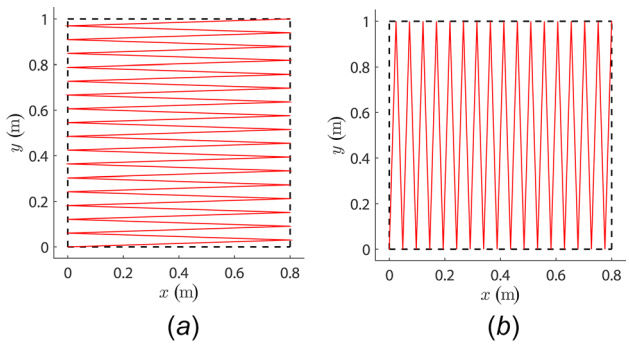

Fig. 2 (*a*) Horizontal scan trajectory (solid lines) and (*b*) a vertical scan trajectory (solid lines) on a rectangular plate (dashed lines)

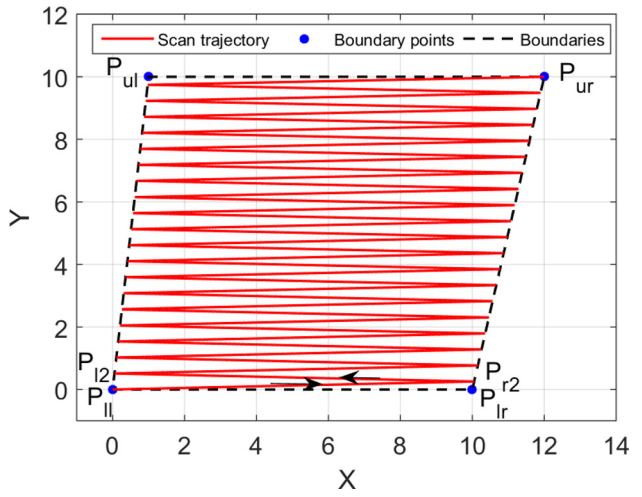

Fig. 3 General quadrangular scan area with a horizontal scan trajectory

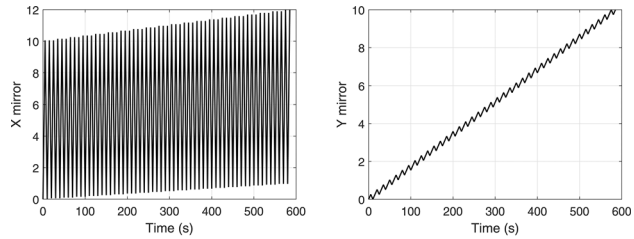

Fig. 4 Voltage signals for the (*a*) *X* and (*b*) *Y* mirrors to generate the scan trajectory in Fig. 3

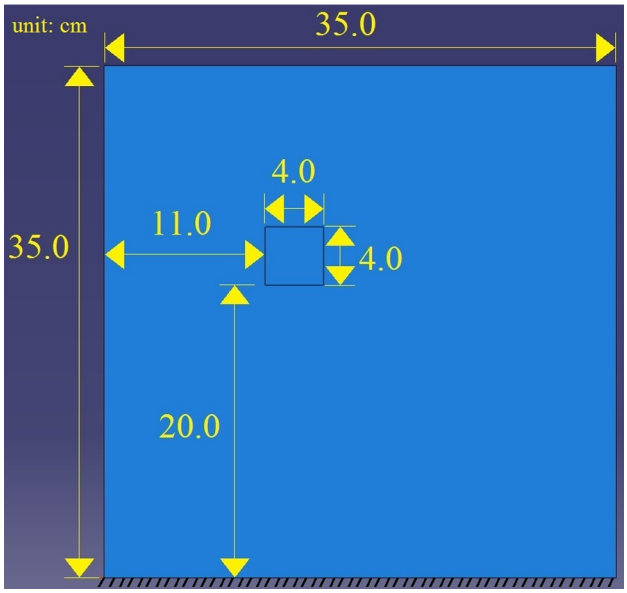

Fig. 5 Dimensions of a six-laminate [0 deg/90 deg/0 deg]$_s$ IM-7 fiber-reinforced polymer composite plate with delamination. The delamination area is a square with the side length of 4.0 cm and located between the third and fourth laminates of the composite plate.

where $k_{\alpha i}$ denotes the constant slope of the scan path associated with the X mirror that can be expressed by

$$k_{\alpha i} = \begin{cases} \dfrac{(\alpha_{lr} + i \times \Delta\alpha_r) - [\alpha_{ll} + (i-1) \times \Delta\alpha_l]}{0.5/f_{\text{scan}}}, & i = 1, 3, \ldots, 2N-1 \\ \dfrac{(\alpha_{ll} + i \times \Delta\alpha_l) - [\alpha_{lr} + (i-1) \times \Delta\alpha_r]}{0.5/f_{\text{scan}}}, & i = 2, 4, \ldots, 2N-2 \end{cases} \tag{35}$$

in which f_{scan} is a scan frequency for each scan path and the duration for an end-to-end scan on a scan path is $0.5/f_{\text{scan}}$. Increments of β from one numbered point to the next on the line $P_{\text{ll}}P_{\text{ul}}$ and the β value for the ith scan path can be expressed by equations similar to those associated with α.

A horizontal scan trajectory in Fig. 3 can be generated using the scanning scheme with voltage signals provided for the X and Y mirrors shown in Figs. 4(*a*) and 4(*b*), respectively; the trajectory is generated with $N = 40$, $M = 3$, and $f_{\text{scan}} = 0.1$ Hz. The total scan time is $(2N-1) \times 0.5 \times M/f_{\text{scan}} = (2 \times 40 - 1) \times 0.5 \times 3/0.1 = 585$ s. Note that the scanning scheme described above can also be used to generate a vertical scan trajectory by swapping the voltage signals for the X and Y mirrors.

The continuous scanning scheme can create a scan trajectory that enables a CSLDV system to obtain a vibration shape on an assigned scan area that is defined by four vertices. Besides a scan area, three parameters N, M, and f_{scan} directly determine densities of scan paths for a scan trajectory and its total scan time. A larger value of N corresponds to a larger number of scan paths and a more spatially detailed description of a vibration shape. A larger value of M can improve the signal-to-noise ratio of a measured vibration shape by averaging measurements of a CSLDV system. It has been shown in Ref. [26] that scanning with f_{scan} smaller than 1 Hz and a large number of averages can enable one to obtain a vibration shape with a high signal-to-noise ratio. Hence, it is recommended that a large value of M and a small value of f_{scan} be used to measure vibration shapes of a plate by a CSLDV system, and a large value of N be used to better describe the vibration shapes.

4 Numerical and Experimental Investigation

4.1 Numerical Investigation. A finite element model of a six-laminate $[0\,\text{deg}/90\,\text{deg}/0\,\text{deg}]_s$ IM-7 fiber reinforced polymer composite plate is constructed to numerically investigate effectiveness of the two delamination identification methods. The composite plate has a delamination area between its third and fourth laminates. Dimensions of the composite plate and delamination area are shown in Fig. 5; the composite plate has a thickness of 0.98 mm. Its mass density is 1545 kg/m^3 and its stiffness matrix is

$$\mathbf{C} = \begin{bmatrix} 286 & 173 & 170.5 & 0 & 0 & 0 \\ 173 & 286 & 170.5 & 0 & 0 & 0 \\ 170.5 & 170.5 & 269.5 & 0 & 0 & 0 \\ 0 & 0 & 0 & 45.3 & 0 & 0 \\ 0 & 0 & 0 & 0 & 45.3 & 0 \\ 0 & 0 & 0 & 0 & 0 & 56.5 \end{bmatrix} \text{GPa} \tag{36}$$

The composite plate has clamped-free-free-free boundary conditions, as shown in Fig. 5, and the clamped boundary is located at its lower boundary. In the finite element model, each laminate is modeled using a total of 350×350 plate elements. Mode shapes

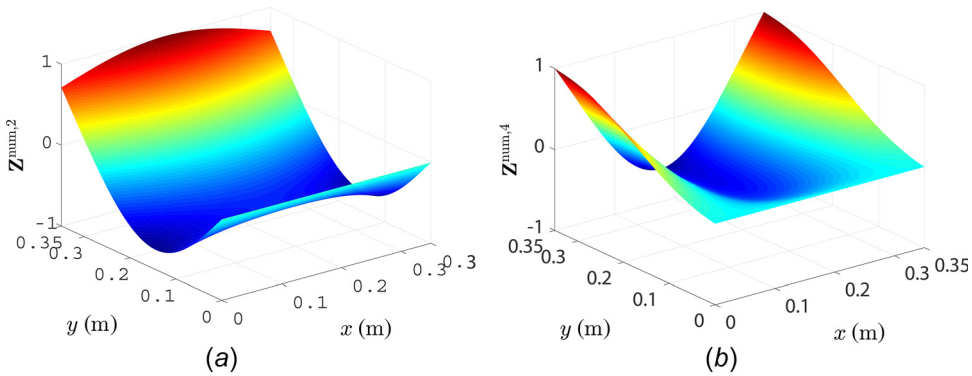

Fig. 6 (*a*) Mode shape of the second out-of-plane mode of the composite plate and (*b*) that of the fourth out-of-plane mode of the plate

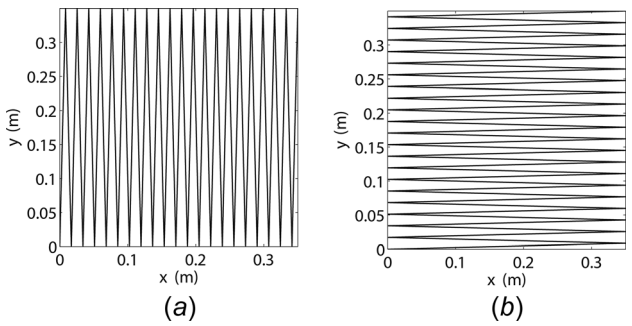

Fig. 7 (*a*) Simulated vertical scan trajectory on the composite plate for $\mathbf{Z}^{\text{num},2}$ and (*b*) the simulated horizontal scan trajectory on the plate for $\mathbf{Z}^{\text{num},4}$

of its second and fourth out-of-plane modes, denoted by $\mathbf{Z}^{\text{num},2}$ and $\mathbf{Z}^{\text{num},4}$, respectively, are calculated and shown in Fig. 6. The mode shapes are normalized so that their maximum amplitudes are one.

Vertical and horizontal scan trajectories with $N = 20$ are assigned to the composite plate. Mode shapes measured by a simulated CSLDV system, denoted by $\mathbf{Z}^{\text{scan},2}$ and $\mathbf{Z}^{\text{scan},4}$, are obtained by interpolating $\mathbf{Z}^{\text{num},2}$ and $\mathbf{Z}^{\text{num},4}$, respectively, along straight scan paths of the trajectories shown in Fig. 7, respectively. In this investigation, $nh = 0.005$ m and $s = 0.005$ m are used to calculate curvature vibration shapes and wavelet transforms of mode shapes, respectively. Curvature damage indices associated with $\mathbf{Z}^{\text{scan},2}$ and $\mathbf{Z}^{\text{scan},4}$ are shown in Figs. 8(*a*) and 8(*b*), respectively, and the associated auxiliary curvature damage index is shown in Fig. 8(*c*). Wavelet damage indices associated with $\mathbf{Z}^{\text{scan},2}$ and $\mathbf{Z}^{\text{scan},4}$ are shown in Figs. 9(*a*) and 9(*b*), respectively, and the associated auxiliary wavelet damage index is shown in Fig. 9(*c*). It can be seen in Figs. 8(*a*) and 9(*a*) that upper and lower edges of the delamination area can be clearly identified; it can be seen in Figs. 8(*b*) and 9(*b*) that left and right edges of the delamination area can be clearly identified. In Figs. 8(*c*) and 9(*c*), four edges of the delamination area can be clearly identified in the auxiliary curvature damage index and auxiliary wavelet damage index, respectively.

4.2 Experimental Investigation. A laminated composite plate with delamination was manufactured using FS-A23 resin and FS-B412 hardener to experimentally investigate effectiveness of the two damage identification methods. Its dimensions and material properties and dimensions of the delamination area were the same as those of the composite plate in the numerical investigation. In the composite plate, a teflon film was embedded between the third and fourth laminates of the composite plate during its manufacturing process to simulate the delamination. A strip area with the width of 2.54 cm adjacent to one boundary of the composite plate was clamped by two aluminum beams with the width of 2.54 cm that were clamped by a bench vice, as shown in Fig. 10(*a*). Since the width of the bench vice jaw was smaller than the side length of the composite plate, the clamping force imposed on the clamped area of the composite plate was not evenly distributed along the length of the clamped area and the clamped boundary condition was imperfect. Since the two damage identification methods intend to identify local anomalies in vibration shapes caused by delamination in composite plates, they can be applicable to composite plates with any boundary conditions, such as the imperfectly clamped boundary in the experiment here, as well as those with nonlinearities.

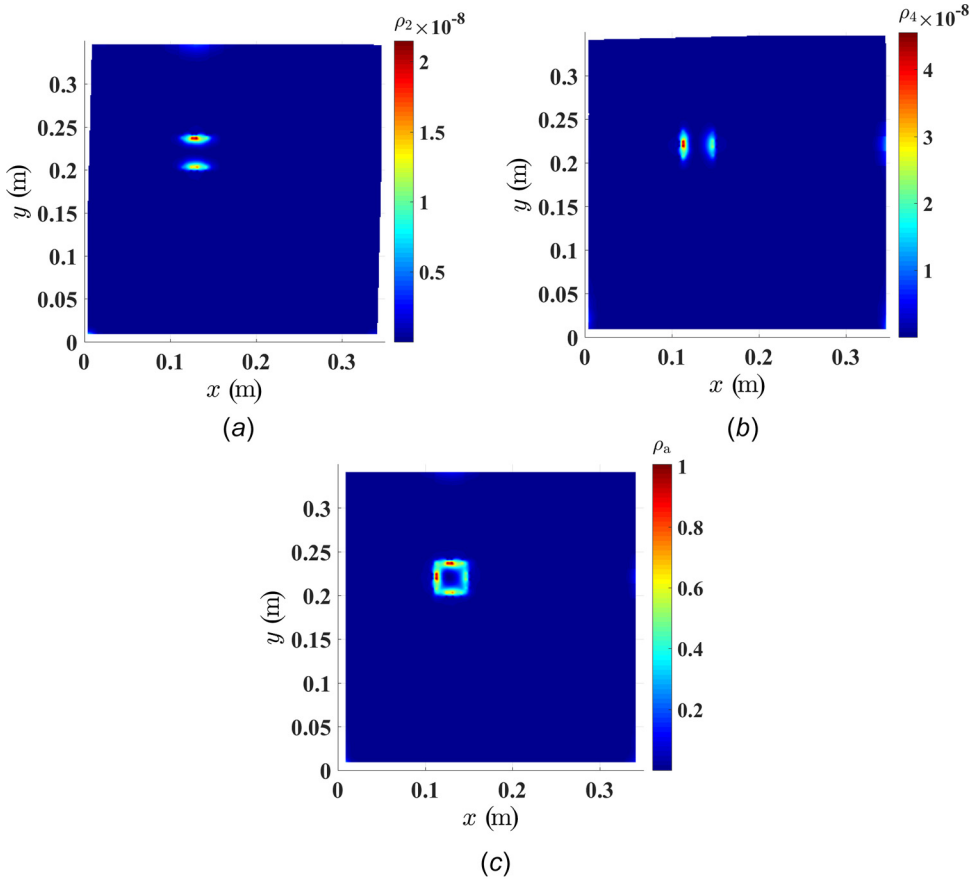

Fig. 8 (*a*) Curvature damage index associated with $\mathbf{Z}^{\text{scan},2}$, (*b*) the curvature damage index associated with $\mathbf{Z}^{\text{scan},4}$, and (*c*) the auxiliary curvature damage index associated with $\mathbf{Z}^{\text{scan},2}$ and $\mathbf{Z}^{\text{scan},4}$; $nh = 0.005$ m is used to calculate curvature vibration shapes

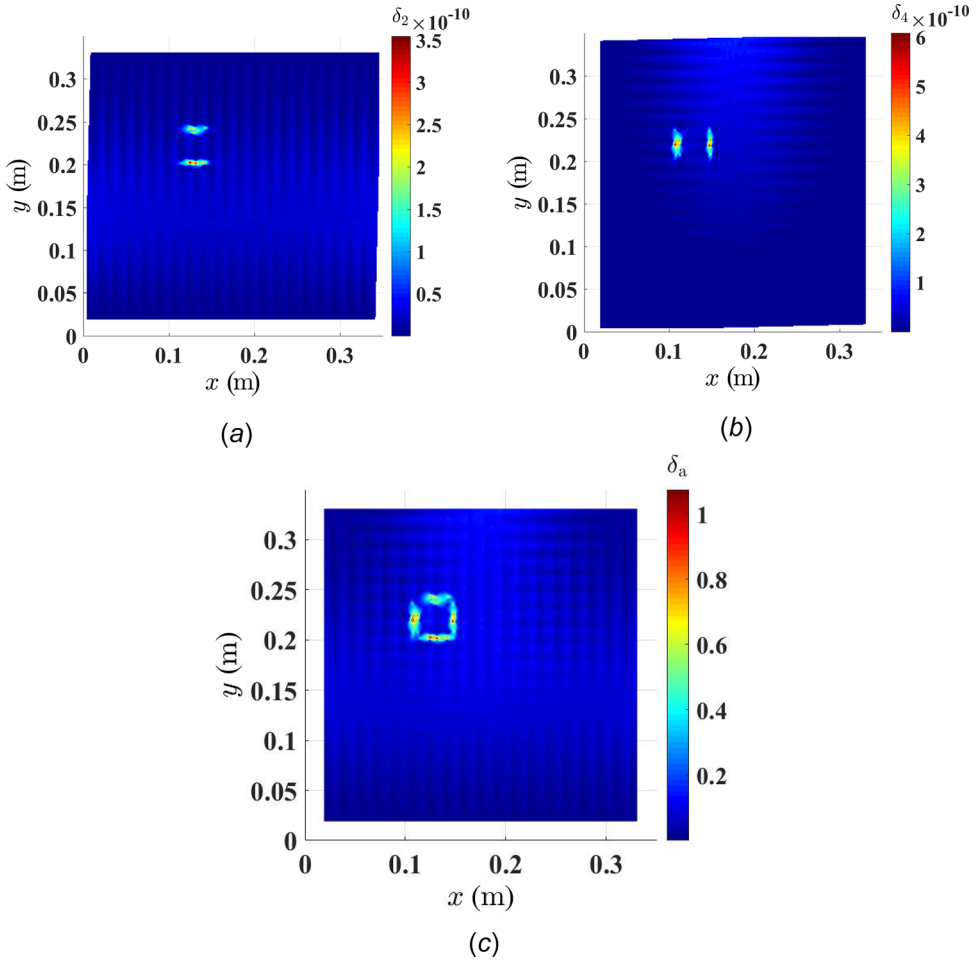

Fig. 9 (*a*) Wavelet damage index associated with $Z^{scan,2}$, (*b*) the wavelet damage index associated with $Z^{scan,4}$, and (*c*) the auxiliary wavelet damage index associated with $Z^{scan,2}$ and $Z^{scan,4}$; $s = 0.005$ m is used to calculate wavelet transforms of mode shapes

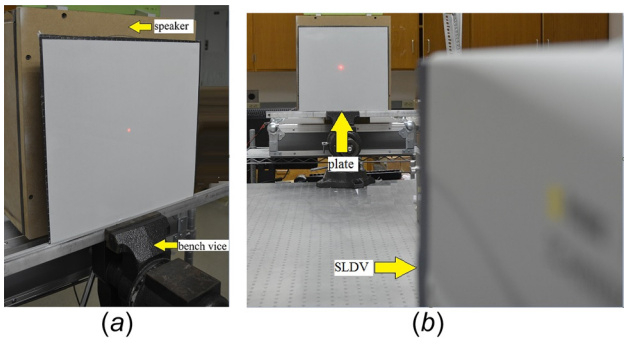

Fig. 10 (*a*) Fixture of the composite plate with delamination and (*b*) the test setup for measurement of vibration shapes of the plate, where "SLDV" stands for scanning laser Doppler vibrometer

The test setup of vibration shape measurement of the composite plate is shown in Fig. 10. A speaker was used to excite the composite plate and a Polytec PSV-500 scanning laser Doppler vibrometer was used to measure its velocity response, which was placed with a relatively long distance from the composite plate. The vibrometer has two key components of the CSLDV system in Fig. 1(*a*), including a single-point laser vibrometer and a scanner. A dSPACE MicroLabBox was connected to the vibrometer to control X and Y mirrors of the scanner. Approximate frequency response functions of the composite plate were measured, with velocity response of the composite plate measured by the vibrometer and a burst chirp signal given to the speaker, which served as response and excitation signals, respectively. There were two peaks at 89 Hz and 150 Hz in a measured frequency response function. Sinusoidal signals with frequencies of 89 Hz and 150 Hz were then given to the speaker to generate acoustic excitation. Vertical and horizontal scan trajectories were assigned on the composite plate to measure its vibration shapes at 89 Hz and 150 Hz, respectively. Vibration shapes at the two frequencies are shown in Fig. 11. Measured vibration shapes at 89 Hz and 150 Hz correspond to the second and fourth modes of the composite plate in its finite element model.

In this experimental investigation, $nh = 0.005$ m and $s = 0.005$ m were used to calculate curvature vibration shapes and wavelet transforms of vibration shapes, respectively. Curvature damage indices associated with vibration shapes at 89 Hz and 150 Hz are shown in Figs. 12(*a*) and 12(*b*), respectively, and the associated auxiliary curvature damage index is shown in Fig. 12(*c*). Wavelet damage indices associated with vibration shapes at 89 Hz and 150 Hz are shown in Figs. 13(*a*) and 13(*b*), respectively, and the associated auxiliary wavelet damage index is shown in Fig. 13(*c*). It can be seen in Figs. 12(*a*) and 13(*a*) that upper and lower edges of the delamination area can be clearly identified; it can be seen in Figs. 12(*b*) and 13(*b*) that left and right edges of the delamination area can be clearly identified. In Figs. 12(*c*) and 13(*c*), four edges of the delamination area can be clearly identified. Delamination identification results from the two methods also compared well with that of a C-scan image of the composite plate shown in

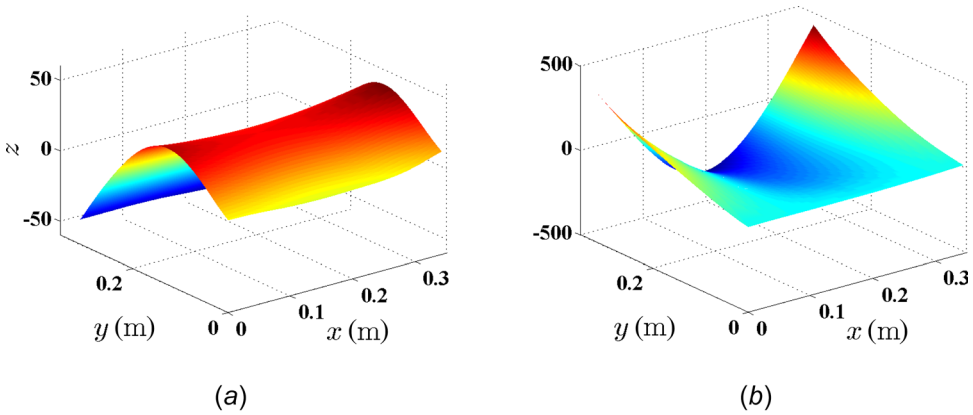

Fig. 11 (*a*) Vibration shape of the composite plate at 89 Hz and (*b*) that of the plate at 150 Hz

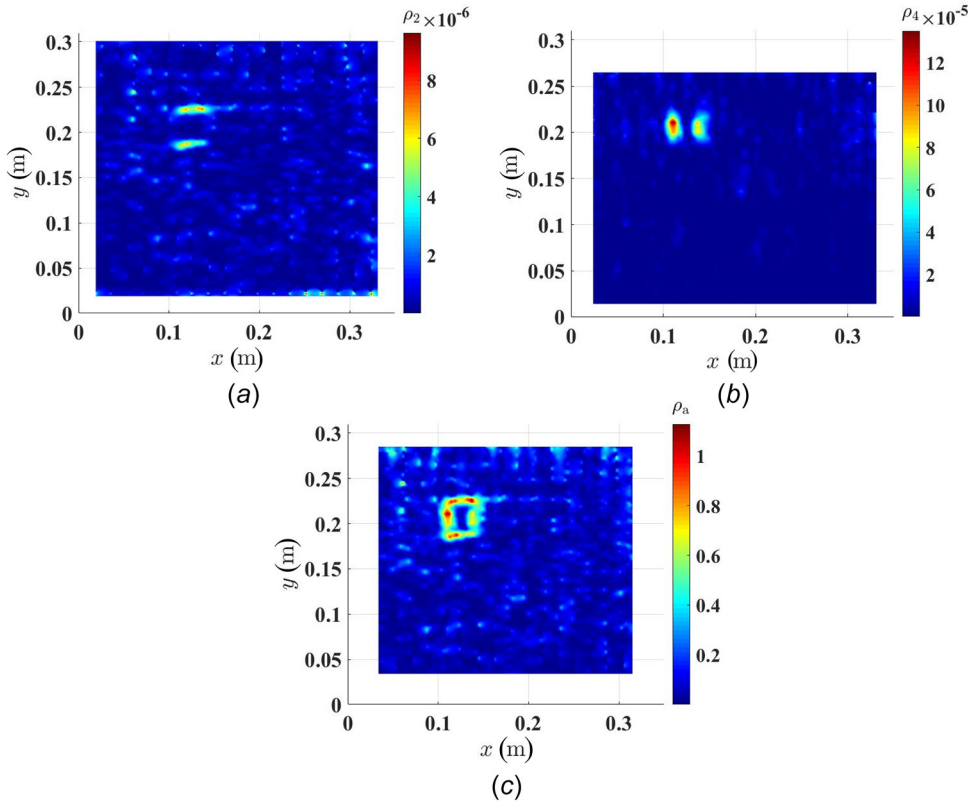

Fig. 12 (*a*) Curvature damage index associated with the mode shape at 89 Hz, (*b*) the curvature damage index associated with the mode shape at 150 Hz, and (*c*) the auxiliary curvature damage index associated with the two mode shapes; *nh* = 0.005 m was used to calculate curvature vibration shapes

Fig. 14. Delamination identification results from the two methods compared well with those from the numerical investigation. Comparing damage identification results from the polynomial-based and wavelet-based methods in Figs. 12 and 13, respectively, one can see that the former has a larger identifiable area than the latter since wavelet transforms can incur severe boundary distortion in associated wavelet damage indices. More importantly, the former yielded the better auxiliary damage index than the latter as a lower level of noise is observed in Fig. 12(*c*).

5 Conclusions

Two non-model-based methods are used to identify delamination in a laminated composite plate using a CSLDV system and their identification results are compared. One is a polynomial-based method that uses polynomial fits to approximate curvature vibration shapes of a corresponding undamaged composite plate and the other is a wavelet-based method that uses continuous wavelet transforms of vibration shapes. In the two methods, local anomalies caused by delamination in curvature vibration shapes are identified in neighborhoods with high damage index values. Auxiliary damage indices associated with curvature damage and wavelet damage indices are formulated, from which positions and lengths of delamination edges can be accurately and completely identified. Both methods do not require any a priori and baseline information of composite plates, such as dimensions, boundary conditions, material properties, and vibration shapes of corresponding undamaged plates. Effectiveness of the two methods has

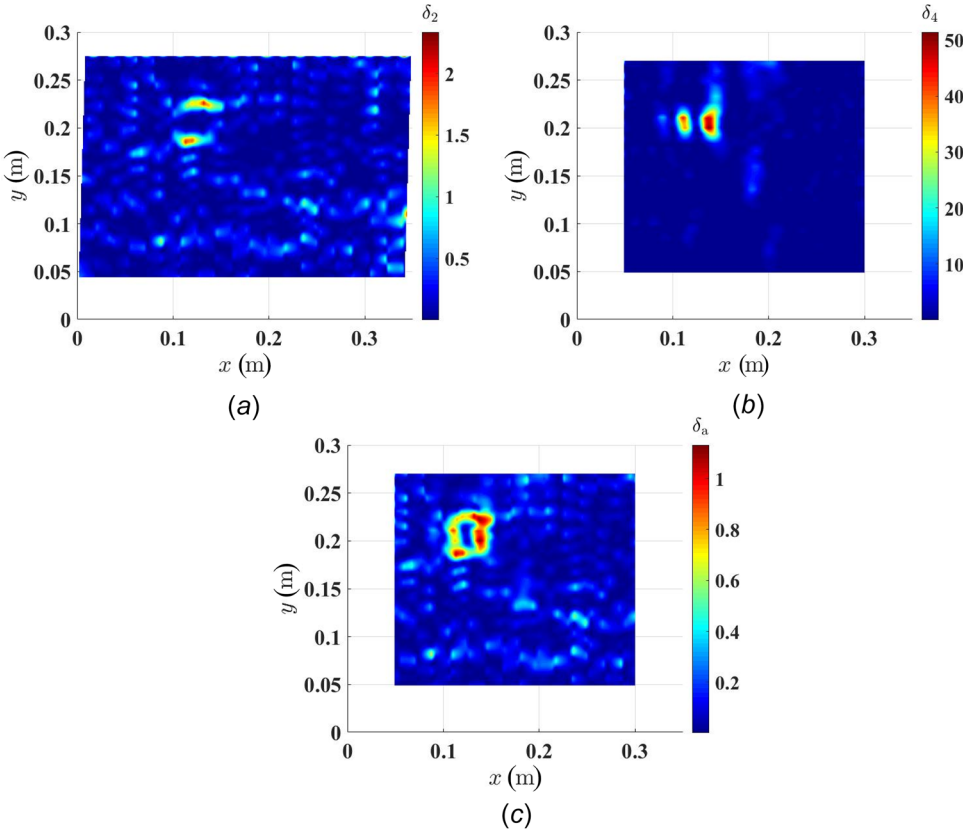

Fig. 13 (*a*) Wavelet damage index associated with the vibration shape at 89 Hz, (*b*) the wavelet damage index associated with the vibration shape at 150 Hz, and (*c*) the auxiliary wavelet damage index associated with the two vibration shapes; $s = 0.005$ m was used to calculate wavelet transforms of vibration shapes

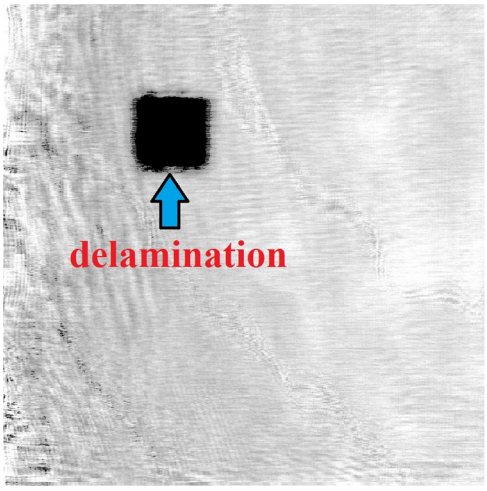

Fig. 14 C-scan image of the composite plate with delamination

been numerically and experimentally investigated to identify delamination in the composite plate. Experimental delamination identification results compare well with that from a C-scan image of the composite plate, and the position and dimensions of the delamination area were accurately and completely identified.

Acknowledgment

The authors would like to thank Professor Aditi Chattopadhyay and Guoyi Li for manufacturing the composite plate used in the experiment and performing a C-scan inspection on the plate.

Funding Data

- Division of Civil, Mechanical and Manufacturing Innovation of the National Science Foundation (Grant Nos. 1229532 and 1335024).
- College of Engineering and Information Technology at the University of Maryland, Baltimore County through a Strategic Plan Implementation Grant.

References

[1] Valdes, S. D., and Soutis, C., 1999, "Delamination Detection in Composite Laminates From Variations of Their Modal Characteristics," J. Sound Vib., **228**(1), pp. 1–9.

[2] Zou, Y., Tong, L., and Steven, G. P., 2000, "Vibration-Based Model-Dependent Damage (Delamination) Identification and Health Monitoring for Composite Structures—A Review," J. Sound Vib., **230**(2), pp. 357–378.

[3] Qiao, P., Lu, K., Lestari, W., and Wang, J., 2007, "Curvature Mode Shape-Based Damage Detection in Composite Laminated Plates," Compos. Struct., **80**(3), pp. 409–428.

[4] Jafari-Talookolaei, R.-A., Abedi, M., and Hajianmaleki, M., 2016, "Vibration Characteristics of Generally Laminated Composite Curved Beams With Single Through-the-Width Delamination," Compos. Struct., **138**, pp. 172–183.

[5] Castro, S. G., and Donadon, M. V., 2017, "Assembly of Semi-Analytical Models to Address Linear Buckling and Vibration of Stiffened Composite Panels With Debonding Defect," Compos. Struct., **160**, pp. 232–247.

[6] Chakraborty, S., Mandal, B., Chowdhury, R., and Chakrabarti, A., 2016, "Stochastic Free Vibration Analysis of Laminated Composite Plates Using Polynomial Correlated Function Expansion," Compos. Struct., **135**, pp. 236–249.

[7] Xu, Y. F., Zhu, W. D., Liu, J., and Shao, Y., 2014, "Identification of Embedded Horizontal Cracks in Beams Using Measured Mode Shapes," J. Sound Vib., **333**(23), pp. 6273–6294.

[8] Xu, W., Zhu, W. D., Smith, S. A., and Cao, M., 2016, "Structural Damage Detection Using Slopes of Longitudinal Vibration Shapes," ASME J. Vib. Acoust., **138**(3), p. 034501.

[9] Lestari, W., Qiao, P., and Hanagud, S., 2007, "Curvature Mode Shape-Based Damage Assessment of Carbon/Epoxy Composite Beams," J. Intell. Mater. Syst. Struct., **18**(3), pp. 189–208.

[10] Yang, Z.-B., Radzienski, M., Kudela, P., and Ostachowicz, W., 2016, "Two-Dimensional Modal Curvature Estimation Via Fourier Spectral Method for Damage Detection," Compos. Struct., **148**, pp. 155–167.
[11] Xu, Y., Zhu, W., and Smith, S., 2017, "Non-Model-Based Damage Identification of Plates Using Principal, Mean and Gaussian Curvature Mode Shapes," J. Sound Vib., **400**, pp. 626–659.
[12] Rothberg, S., Baker, J., and Halliwell, N. A., 1989, "Laser Vibrometry: Pseudo-Vibrations," J. Sound Vib., **135**(3), pp. 516–522.
[13] Sriram, P., Hanagud, S., Craig, J., and Komerath, N., 1990, "Scanning Laser Doppler Technique for Velocity Profile Sensing on a Moving Surface," Appl. Opt., **29**(16), pp. 2409–2417.
[14] Sriram, P., Hanagud, S., and Craig, J., 1992, "Mode Shape Measurement Using a Scanning Laser Doppler Vibrometer," Int. J. Anal. Exp. Modal Anal., **7**(3), pp. 169–178.
[15] Stanbridge, A., and Ewins, D., 1996, "Using a Continuously-Scanning Laser Doppler Vibrometer for Modal Testing," 14th International Modal Analysis Conference (IMAC), Dearborn, MI, pp. 816–822.
[16] Stanbridge, A., and Ewins, D., 1999, "Modal Testing Using a Scanning Laser Doppler Vibrometer," Mech. Syst. Signal Process., **13**(2), pp. 255–270.
[17] Stanbridge, A., Ewins, D., and Khan, A., 2000, "Modal Testing Using Impact Excitation and a Scanning LDV," Shock Vib., **7**(2), pp. 91–100.
[18] Stanbridge, A., Martarelli, M., and Ewins, D., 1999, "The Scanning Laser Doppler Vibrometer Applied to Impact Modal Testing," Proc. SPIE **3411**, pp. 986–991.
[19] Di Maio, D., and Ewins, D., 2011, "Continuous Scan, a Method for Performing Modal Testing Using Meaningful Measurement Parameters—Part I," Mech. Syst. Signal Process., **25**(8), pp. 3027–3042.
[20] Allen, M. S., and Sracic, M. W., 2010, "A New Method for Processing Impact Excited Continuous-Scan Laser Doppler Vibrometer Measurements," Mech. Syst. Signal Process., **24**(3), pp. 721–735.
[21] Chen, D.-M., Xu, Y. F., and Zhu, W. D., 2016, "Damage Identification of Beams Using a Continuously Scanning Laser Doppler Vibrometer System," ASME J. Vib. Acoust., **138**(5), p. 051011.
[22] Xu, Y. F., Chen, D.-M., and Zhu, W. D., 2017, "Damage Identification of Beam Structures Using Free Response Shapes Obtained by Use of a Continuously Scanning Laser Doppler Vibrometer System," Mech. Syst. Signal Process., **92**, pp. 226–247.
[23] Timoshenko, S. P., and Woinowsky-Krieger, S., 1959, *Theory of Plates and Shells*, McGraw-Hill, New York.
[24] Cox, I., and Gaudard, M., 2013, *Discovering Partial Least Squares With JMP*, SAS Institute, Cary, NC.
[25] Mallat, S., 1999, *A Wavelet Tour of Signal Processing*, Academic Press, Burlington, MA.
[26] Chen, D.-M., Xu, Y. F., and Zhu, W. D., 2017, "Experimental Investigation of Notch-Type Damage Identification With a Curvature-Based Method by Using a Continuously Scanning Laser Doppler Vibrometer System," J. Nondestr. Eval., **36**(2), p. 38.